

# PARTICLE PRODUCTION IN THE CENTRAL REGION AT LHC ENERGIES

C. Merino\*, C. Pajares\*, and Yu.M. Shabelski\*\*

\* Departamento de Física de Partículas, Facultade de Física,  
and Instituto Galego de Física de Altas Enerxías (IGFAE),  
Universidade de Santiago de Compostela,  
E-mail: merino@fpaxp1.usc.es  
E-mail: pajares@fpaxp1.usc.es

\*\* Petersburg Nuclear Physics Institute,  
E-mail: shabelsk@thd.pnpi.spb.ru

*Contribution to the Proceedings of Low-x Meeting 2011  
Santiago de Compostela, Galice, Spain, 3<sup>d</sup>-7<sup>th</sup> June 2011*

*Talk presented by Yu.M. Shabelski*

## A b s t r a c t

We consider the first LHC data for  $pp$  collisions in the framework of Regge phenomenology, and the Quark-Gluon String Model, and we present the corresponding predictions for both the integral cross sections and the inclusive densities of secondaries, that are determined by Pomeron exchange. All parameters were fixed long time ago for the description of the data at fixed target energies. The first measurements of the total inelastic cross section by ATLAS and CMS Collaborations are in agreement with our calculations. Also the inclusive densities measured in the central region are in agreement with our theoretical predictions on the accuracy level of about 10–15%.

# 1 Introduction

In Regge theory the Pomeron exchange dominates the high energy soft hadron interaction, the contributions of all other exchanges to the total or inelastic cross sections becoming negligibly small at LHC energies.

The Quark-Gluon String Model (QGSM) [1] is based on Dual Topological Unitarization (DTU), Regge phenomenology, and nonperturbative notions of QCD. This model is successfully used for the description of multiparticle production processes in hadron-hadron [2, 3, 4, 5, 6, 7, 8], hadron-nucleus [9, 10], and nucleus-nucleus [11] collisions. In particular, the inclusive densities of different secondaries produced in  $pp$  collisions at  $\sqrt{s} = 200$  GeV in midrapidity region were reasonably described in ref. [6] (see also refs. [7, 8]).

In the QGSM high energy interactions are considered as proceeding via the exchange of one or several Pomerons, and all elastic and inelastic processes result from cutting through or between Pomerons [12]. Inclusive spectra of hadrons are related to the corresponding fragmentation functions of quarks and diquarks, which are constructed using the Reggeon counting rules [13]. The quantitative predictions of the QGSM depend on the values of several parameters that were fixed at once by the comparison of the corresponding calculations to the experimental data obtained at fixed target energies.

The experimental data obtained at LHC allow us to test the stability of the QGSM predictions and of the values of the model parameters. Fortunately, one can see that the model predictions are in reasonable agreement with the first LHC data.

In this paper we discuss the cross sections, inclusive densities of secondaries, and the antibaryon/baryon ratios at LHC energies in the framework of QGSM.

## 2 Cross sections

For the Pomeron trajectory

$$\alpha_P(t) = 1 + \Delta + \alpha'_P \cdot t, \quad \Delta > 0, \quad (1)$$

the one-Pomeron contribution to  $\sigma_{hN}^{tot}$  equals

$$\sigma_P = 8\pi \cdot \gamma \cdot e^{\Delta \cdot \xi}, \quad \text{with } \xi = \ln s/s_0, \quad (2)$$

where  $\gamma = g_1(0) \cdot g_2(0)$  is the Pomeron coupling,  $s_0 \simeq 1 \text{ GeV}^2$ , and  $\sigma_P$  rises with energy as  $s^\Delta$ . The correct asymptotic behavior  $\sigma_{hN}^{tot} \sim \ln^2 s$ , compatible with the Froissart

bound [14], can be obtained by taking into account the multipomeron exchanges in the diagrams of Fig. 1.

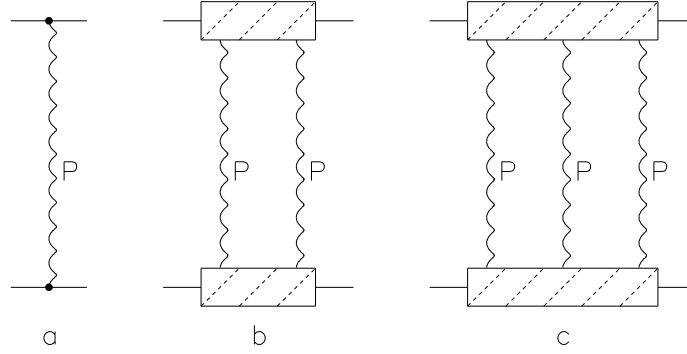


Figure 1: Regge-pole theory diagrams: (a) single, (b) double, (c) and triple Pomeron exchange in elastic  $hN$  scattering. The hadron couplings to two and three Pomerons are shown by dashed boxes.

A simple quasi-eikonal treatment [15] yields to

$$\sigma_{hN}^{tot} = \sigma_P \cdot f(z/2), \quad \sigma_{hN}^{el} = \frac{\sigma_P}{C} \cdot [f(z/2) - f(z)], \quad (3)$$

$$f(z) = \sum_{k=1}^{\infty} \frac{1}{k \cdot k!} \cdot (-z)^{k-1} = \frac{1}{z} \int_0^z \frac{dx}{x} \cdot (1 - e^{-x}), \quad (4)$$

$$z = \frac{2C \cdot \gamma}{\lambda} \cdot e^{\Delta\xi}, \quad \lambda = R^2 + \alpha'_P \cdot \xi. \quad (5)$$

Here,  $R^2$  is the radius of the Pomeron and  $C$  is the quasi-eikonal enhancement coefficient.

At asymptotically high energies ( $z \gg 1$ ) we obtain

$$\sigma_{hN}^{tot} = \frac{8\pi \cdot \alpha'_P \cdot \Delta}{C} \cdot \xi^2, \quad \sigma_{hN}^{el} = \frac{4\pi \cdot \alpha'_P \cdot \Delta}{C^2} \cdot \xi^2, \quad (6)$$

according to the Froissart limit [14].

The numerical values of the Pomeron parameters were taken [3] to be :

$$\Delta = 0.139, \quad \alpha'_P = 0.21 \text{ GeV}^{-2}, \quad \gamma = 1.77 \text{ GeV}^{-2}, \quad R^2 = 3.18 \text{ GeV}^{-2}, \quad C = 1.5. \quad (7)$$

The predictions of Regge theory obtained with these values of the parameters (and accounting for a small contribution from non-Pomeron exchange) are presented in Table. 1.

$\sqrt{s}$	$\sigma^{tot}$	$\sigma^{el}$	$\sigma^{inel}$	$\sigma^{inel}(\text{ATLAS [16]})$	$\sigma^{inel}(\text{CMS [17]})$
900 GeV	67.4	13.2	54.2	$69.4 \pm 2.4$	66.8 - 74.8
7 TeV	94.5	21.1	73.4		
14 TeV	105.7	24.2	81.5		

Table 1. The Regge theory predictions for total, total elastic, and total inelastic cross sections (in mb) in  $pp$  collisions at LHC energies.

These results are in agreement with those in ref. [18].

The experimental points for  $\sigma_{pp}^{inel}$  measured by ATLAS and CMS Collaboration [16, 17] presented in Table 1 (we omit the error bar coming from extrapolation) are in a reasonable agreement with our calculations.

However, in the complete Reggeon diagram technique [19] not only Regge-poles and cuts but also more complicated diagrams (e.g. the so-called enhanced diagrams) should be taken into account. In the numerical calculations of such diagrams some new uncertainties appear due to the fact that the vertices of the coupling of  $n$  and  $m$  Reggeons are unknown.

The numerical calculations which account for enhanced diagrams [20, 21, 22] lead the values of  $\sigma_{pp}^{inel}$  of the same order ( $\pm 10\%$  at  $\sqrt{s} = 14$  TeV) as those presented in Table 1. The values of  $\sigma_{pp}^{inel}$  calculated in refs. [20, 21] are slightly smaller than the experimental values [16, 17], and while two sets of calculations in ref. [22] lead to too large cross section, the third one [22] practically coincides with our results.

### 3 Inclusive densities

The Quark-Gluon String Model (QGSM) [1, 2, 3] allows us to make quantitative predictions of different features of multiparticle production, in particular, the inclusive densities of different secondaries both in the central and in the beam fragmentation regions. In QGSM high energy hadron-nucleon collisions are considered as taking place via the exchange of one or several Pomerons, all elastic and inelastic processes resulting from cutting through or between Pomerons [12].

Each Pomeron corresponds to a cylindrical diagram (see Fig. 2a), and thus, when cutting one Pomeron, two showers of secondaries are produced as it is shown in Fig. 2b. The inclusive spectrum of a secondary hadron  $h$  is then determined by the convolution of the diquark, valence quark, and sea quark distributions  $u(x, n)$  in the incident particles, with the fragmentation functions  $G^h(z)$  of quarks and diquarks into the secondary

hadron  $h$ . These distributions, as well as the fragmentation functions, are constructed by using the Reggeon counting rules [13]. Both the diquark and the quark distribution functions depend on the number  $n$  of cut Pomerons in the considered diagram.

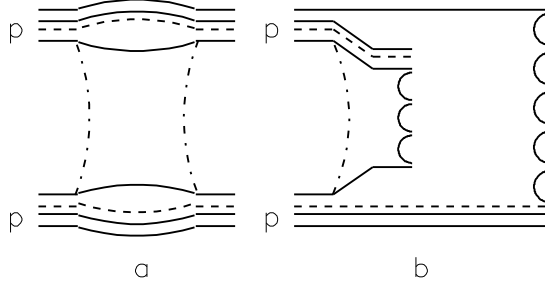


Figure 2: (a) Cylindrical diagram corresponding to the one-Pomeron exchange contribution to elastic  $pp$  scattering, and (b) the cut of this diagram which determines the contribution to the inelastic  $pp$  cross section. Quarks are shown by solid curves and string junction by dashed curves.

For a nucleon target, the inclusive rapidity  $y$  (or Feynman- $x$   $x_F$ ) spectrum of a secondary hadron  $h$  has the form [1]:

$$\frac{dn}{dy} = \frac{x_E}{\sigma_{inel}} \cdot \frac{d\sigma}{dx_F} = \frac{dn}{dy} = \sum_{n=1}^{\infty} w_n \cdot \phi_n^h(x) + w_D \cdot \phi_D^h(x) , \quad (8)$$

where the functions  $\phi_n^h(x)$  determine the contribution of the diagram with  $n$  cut Pomerons and  $w_n$  is the relative weight of this diagram. The last term  $w_D \cdot \phi_D^h(x)$  accounts for the contribution of diffraction dissociation processes.

For  $pp$  collisions

$$\begin{aligned} \phi_{pp}^h(x) &= f_{qq}^h(x_+, n) \cdot f_q^h(x_-, n) + f_q^h(x_+, n) \cdot f_{qq}^h(x_-, n) + \\ &+ 2 \cdot (n-1) \cdot f_s^h(x_+, n) \cdot f_s^h(x_-, n) , \end{aligned} \quad (9)$$

$$x_{\pm} = \frac{1}{2} \cdot \left[ \sqrt{4m_T^2/s + x^2} \pm x \right] , \quad (10)$$

where  $f_{qq}$ ,  $f_q$ , and  $f_s$  correspond to the contributions of diquarks, valence quarks, and sea quarks, respectively.

These functions are determined by the convolution of the diquark and quark distributions (that are normalized to one) with the fragmentation functions, e.g. for the quark one can write:

$$f_q^h(x_+, n) = \int_{x_+}^1 u_q(x_1, n) \cdot G_q^h(x_+/x_1) dx_1 . \quad (11)$$

At very high energies both  $x_+$  and  $x_-$  are negligibly small in the midrapidity region, and so all fragmentation functions, which are usually written [13] as  $G_q^h(z) = a_h \cdot (1-z)^\beta$ , become constants and equal for a particle and its antiparticle:

$$G_q^h(x_+/x_1) = a_h . \quad (12)$$

This leads, in agreement with [23], to

$$\frac{dn}{dy} = g_h \cdot (s/s_0)^{\alpha_P(0)-1} \sim a_h^2 \cdot (s/s_0)^{\alpha_P(0)-1} , \quad (13)$$

that corresponds to the only one-Pomeron exchange diagram (AGK theorem [12]) at asymptotically high energy. The values of the Pomeron parameters presented in Eq. (7) are used in the QGSM numerical calculations.

The values  $dn/dy$  in the central region can be obtained under different conditions. Sometimes they are presented for all inelastic interactions, while in other cases they correspond to the events without single diffraction (NSD), or to events called INEL $> 0$ , in which as minimum one charged particle should be detected in the kinematical window  $|\eta| > 1$  [25]. When considering the experimental value  $dn/dy = N_{particles}/N_{events}$  one has to keep in mind that though for both NSD and INEL $> 0$  triggers the value of  $N_{particles}$  in midrapidity region at LHC energies is constant, the number of events  $N_{events}$  significantly changes in these three cases, leading to different values of  $dn/dy$ .

As an example, we present in Table 2 three values of  $dn/dy$  measured by the ALICE Collaboration [24, 25, 26] at  $\sqrt{s} = 900$  GeV.

	All inelastic [24]	NSD [24]	INEL $> 0$ [25, 26]
dn/dy	$3.02 \pm 0.01_{0.05}^{0.08}$	$3.58 \pm 0.01_{0.12}^{0.12}$	$3.81 \pm 0.01_{0.07}^{0.07}$

Table 2. The inclusive densities of charged secondaries measured by ALICE Collaboration in all inelastic events, in events without single diffraction (NSD), and in events with as minimum one charged particle in the kinematical window  $|\eta| > 1$  (INEL $> 0$ ), in  $pp$  collisions at  $\sqrt{s} = 900$  GeV [24, 25, 26].

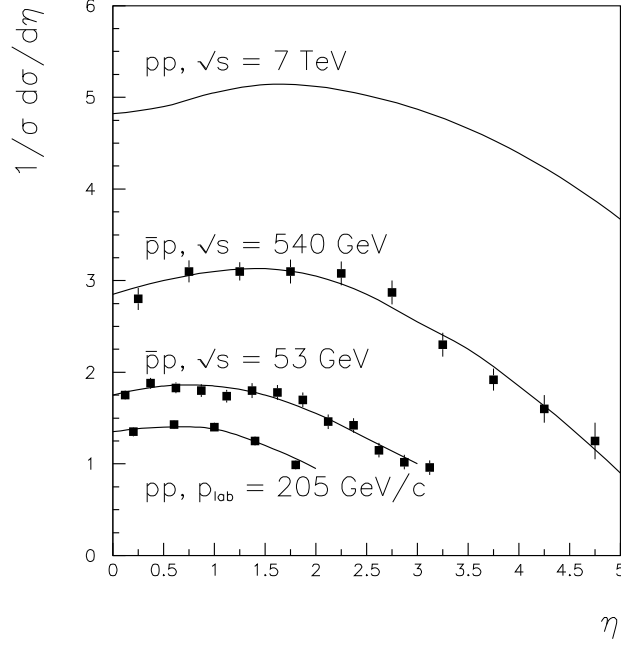


Figure 3: The QGSM predictions for the pseudorapidity distributions of all charged secondaries produced in inelastic  $pp$  and  $\bar{p}p$  collisions at different energies.

The QGSM predictions for the  $dn/d\eta$  distributions of all charged secondaries produced in inelastic  $pp$  and  $\bar{p}p$  collisions at different energies are shown in Fig. 3. The experimental data are taken from ref. [27].

The QGSM allows one to calculate the inclusive spectra of different secondaries. The comparison of our predictions [8] with new data by the ALICE Collaboration [28] is presented in Table 3.

Particle	QGSM [8]	ALICE Collaboration [28]
$\pi^+$	1.68	$1.493 \pm 0.004 \pm 0.074$
$\pi^-$	1.66	$1.485 \pm 0.004 \pm 0.074$
$K^+$	0.17	$0.184 \pm 0.004 \pm 0.015$
$K^-$	0.16	$0.183 \pm 0.004 \pm 0.015$
$\bar{p}$	0.10	$0.077 \pm 0.002 \pm 0.006$
$\bar{\Lambda}$	0.05	0.08
$\bar{\Xi}^+$	0.005	0.009
$\bar{\Omega}^+$	0.0004	0.0008

Table 3. The QGSM predictions [8] for the midrapidity yields  $dn/dy$  ( $|y| < 0.5$ ) of different secondaries.

daries at energy  $\sqrt{s} = 900$  GeV together with the corresponding experimental data by the ALICE Collaboration [28].

The inclusive densities of pions are slightly overestimated. The predicted [8] value of the ratio of  $\Xi^-/\Lambda$  midrapidity yields ( $\sim 0.10$ ) is in agreement with the experimental result [29]  $\Xi^-/\Lambda \simeq 0.11 \pm 0.005$ . The agreement of the order of 10–15% for all cases can be considered as a reasonable one.

We predict [8] for all inelastic interactions one increase of the midrapidity yields for  $\pi$  and  $K$  mesons of about 1.4 times in the energy region  $\sqrt{s} = 900$  GeV–7 TeV (smaller than the increase in the data [30] for  $K_s^0$  equal to  $1.69 \pm 0.01 \pm 0.06$  in NSD events). For antibaryons we predict [8] increases from  $\sim 1.6$  for  $\bar{p}$  and  $\bar{\Lambda}$  to  $\sim 2.0$  for  $\bar{\Omega}$ .

## 4 Baryon/antibaryon asymmetry in QGSM

In the string models baryons are considered as configurations consisting of three connected strings (related to three valence quarks) called string junction (SJ) [31, 32, 33, 34], as it is shown in Fig. 4. Such a baryon structure is supported by lattice calculations [35].

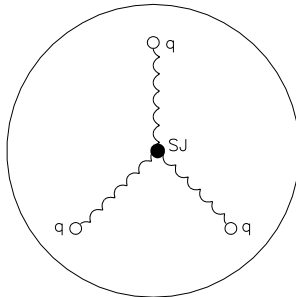


Figure 4: The composite structure of a baryon in string models. Quarks are shown by open points and SJ by black point.

This picture leads to some general phenomenological predictions. In particular, it opens room for exotic states, such as the multiquark bound states, 4-quark mesons, and pentaquarks [33, 36, 37]. In the case of inclusive reactions, the baryon number transfer to large rapidity distances in hadron-nucleon reactions can be explained [5] by SJ diffusion.



The production of a baryon-antibaryon pair in the central region usually occurs via  $SJ\text{-}\overline{SJ}$  pair production. Then, the SJ, that has upper color indices, combines with sea quarks, while the antiSJ ( $\overline{SJ}$ ), that has lower indices, combines with sea antiquarks, resulting, respectively, into the  $B$  and the  $\bar{B}$  of a  $B\bar{B}$  pair [33, 38], as it is shown in Figure 5a.

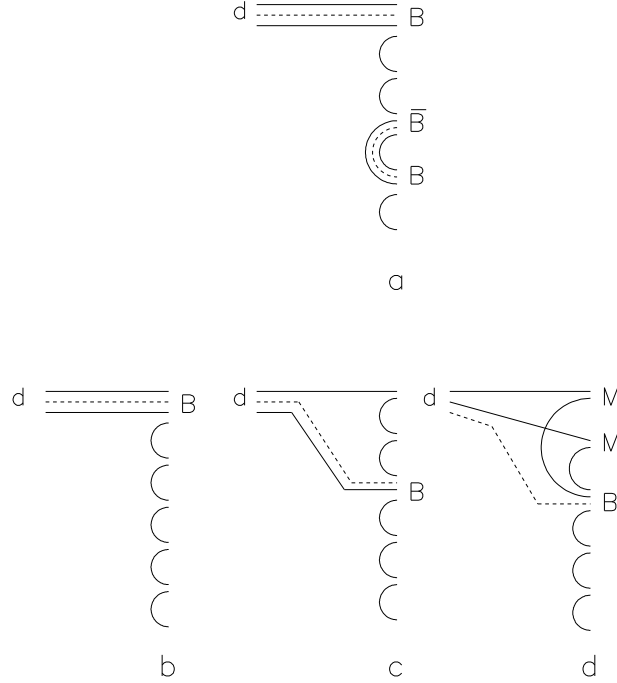


Figure 5: QGSM diagrams describing secondary baryon  $B$  production by diquark  $d$ . (a) Central production of  $\bar{B}B$  pair via production of new  $SJ\text{-}\overline{SJ}$  pair. Single production of  $B$  in the processes of diquark fragmentation: (b) initial  $SJ$  together with two valence quarks and one sea quark, (c) initial  $SJ$  together with one valence quark and two sea quarks, and (d) initial  $SJ$  together with three sea quarks. Quarks are shown by solid curves and  $SJ$  by dashed curves.

In processes with incident baryons, e.g. in  $pp$  collisions, another possibility to produce a secondary baryon in the central region exists. This second possibility is connected with the diffusion in rapidity space of a  $SJ$  existing in the initial state and it leads to significant differences in the yields of baryons and antibaryons in the midrapidity region even at rather high energies [5]. Probably, the most important experimental fact in favour for this process is the rather large asymmetry in  $\Omega$  and  $\bar{\Omega}$  baryon production in high energy  $\pi^-p$  interactions [39].

The quantitative theoretical description of the baryon number transfer via  $SJ$  mechanism was suggested in the 90's and used to predict [40] the  $p/\bar{p}$  asymmetry at HERA

energies. The quantitative description of the baryon number transfer due to SJ diffusion in rapidity space was first obtained in [5] and then in papers [6, 7, 8, 41, 42, 43].

To obtain the net baryon charge we consider three different possibilities according to ref. [5]. The first one is the fragmentation of the incoming diquark giving rise to a leading baryon (Figure 5b). A second possibility is to produce a leading meson in the first break-up of the string and one baryon in a subsequent break-up (Figure 5c). In these two first cases the baryon number transfer is possible only for short distances in rapidity. In the third case, shown in Figure 5d, both initial valence quarks in the diquark recombine with sea antiquarks into mesons  $M$ , while a secondary baryon is formed by the SJ together with three sea quarks.

The fragmentation functions for the secondary baryon  $B$  production corresponding to the three processes shown in Figs. 5b-d can be written as follows (see [5] for more details):

$$G_{qq}^B(z) = a_N \cdot v_{qq}^B \cdot z^{2.5} , \quad (14)$$

$$G_{qs}^B(z) = a_N \cdot v_{qs}^B \cdot z^2 \cdot (1 - z) , \quad (15)$$

$$G_{ss}^B(z) = a_N \cdot \varepsilon \cdot v_{ss}^B \cdot z^{1-\alpha_{SJ}} \cdot (1 - z)^2 , \quad (16)$$

for Figs. 5b, 5c, and 5d, respectively, and where  $a_N$  is the normalization parameter that was determined from the experimental data at fixed target energies, and  $v_{qq}^B$ ,  $v_{qs}^B$ ,  $v_{ss}^B$  are the relative probabilities for different baryons production that can be found by simple quark combinatorics [44, 45].

The contribution shown in Figure 5d is essential if the intercept of the SJ exchange Regge-trajectory,  $\alpha_{SJ}$ , is large enough. The contribution of the graph in Figure 5d is weighted in QGSM by the coefficient  $\varepsilon$  which determines the small probability for such a baryon number transfer to occur. Let's finally note that this process can be very naturally realized in the quark combinatorial approach [44] through the specific probabilities of a valence quark recombination (fusion) with sea quarks and antiquarks.

At high energies the SJ contribution to the inclusive cross section of secondary baryon production at large rapidity distance  $\Delta y$  from the incident nucleon can be estimated as

$$\frac{1}{\sigma} \cdot \frac{d\sigma^B}{dy} \sim a_B \cdot \varepsilon \cdot e^{-(1-\alpha_{SJ}) \cdot \Delta y} , \quad (17)$$

where  $a_B = a_N \cdot v_{ss}^B$ .

The data by the ALICE Collaboration [46] for  $\bar{p}/p$  ratios in  $pp$  collisions at LHC energies  $\sqrt{s} = 900$  GeV and 7 TeV are presented in Table 4, together with QGSM the corresponding calculations with different values of  $\alpha_{SJ}$ . These data seem to favour the

value  $\alpha_{SJ} = 0.5$ , what could mean that the Odderon contribution is not seen [7] in this process.

SJ exchange	$\sqrt{s} = 900 \text{ GeV}$	$\sqrt{s} = 7 \text{ TeV}$
$\alpha_{SJ} = 0.9$	0.89	0.95
$\alpha_{SJ} = 0.5$	0.95	0.99
$\varepsilon = 0$	0.98	1.
ALICE [46]	$0.957 \pm 0.006 \pm 0.014$	$0.991 \pm 0.005 \pm 0.014$

Table 4. The QGSM predictions for  $\bar{p}/p$  in  $pp$  collisions at LHC energies and the data by the ALICE Collaboration [46]. The value  $\varepsilon = 0$  corresponds to the case with not C-negative exchange.

The LHCb Collaboration measured the ratios of  $\bar{\Lambda}$  to  $\Lambda$  in the rapidity interval  $2 < y < 4$  at  $\sqrt{s} = 900 \text{ GeV}$  and 7 TeV [47]. We compare these results with the QGSM calculations in Fig. 6.

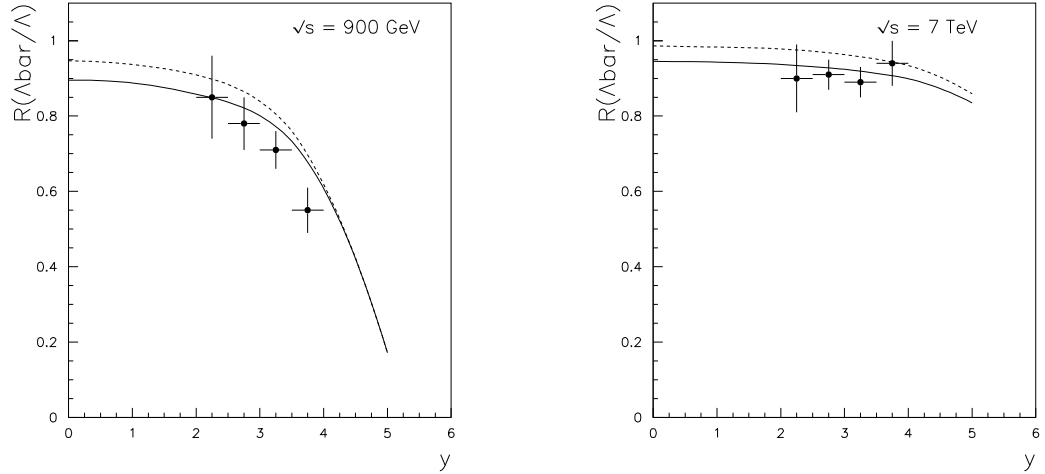


Figure 6: The QGSM predictions (solid curves for  $\alpha_{SJ} = 0.9$  and dashed curves for  $\alpha_{SJ} = 0.5$ ) for the ratios of the spectra of secondary  $\bar{\Lambda}$  to  $\Lambda$  as the functions of their rapidities at energies  $\sqrt{s} = 900 \text{ GeV}$  (left) and  $\sqrt{s} = 7 \text{ TeV}$  (right), together with the experimental data by the LHCb Collaboration [47].

One can see that here the QGSM calculation with the value  $\alpha_{SJ} = 0.9$  is in a slightly better agreement with the data. It is also necessary to note that the predictions of

PYTHIA 6 MC generator are in disagreement with the experimental data at  $\sqrt{s} = 900$  GeV.

We predict practically equal  $\overline{B}/B$  ratios for baryons with different strangeness content.

## 5 Conclusion

The first experimental data obtained at LHC are in general agreement with the calculations provided by QGSM in the framework of Regge theory with the same values of parameters that were determined at lower energies (mainly for the description of the data of fixed target experiments).

We neglect the possibility of interactions between Pomerons (so-called enhancement diagrams) in the calculations of integrated cross sections and inclusive densities. Such interactions are very important in the cases of heavy ion [48] and nucleon-nucleus [49] interactions at RHIC energies, and their contribution should increase with energy. However, we estimate [49] that the contributions of these enhanced diagrams to the inclusive density of secondaries produced in  $pp$  collisions at LHC energies is not large enough to be significant.

### Acknowledgements

We are grateful to A.B. Kaidalov for useful discussions and comments. This paper was supported by Ministerio de Educación y Ciencia of Spain under the Spanish Consolider-Ingenio 2010 Programme CPAN (CSD2007-00042), by Xunta de Galicia project FPA 2005–01963, and, in part, by grant RSGSS-3628.2008.2.

## References

- [1] A.B. Kaidalov and K.A. Ter-Martirosyan, *Yad. Fiz.* **39**, 1545 (1984); **40**, 211 (1984).
- [2] A.B. Kaidalov and O.I. Piskounova, *Yad. Fiz.* **41**, 1278 (1985); *Z. Phys.* **C30**, 145 (1986).
- [3] Yu.M. Shabelski, *Yad. Fiz.* **44**, 186 (1986).
- [4] F. Anselmino, L. Cifarelli, E. Eskut, and Yu.M. Shabelski, *Nouvo Cim.* **105A**, 1371 (1992).

- [5] G.H. Arakelyan, A. Capella, A.B. Kaidalov, and Yu.M. Shabelski, Eur. Phys. J. C **26**, 81 (2002) and hep-ph/0103337.
- [6] G.H. Arakelyan, C. Merino, C. Pajares, and Yu.M. Shabelski, Eur. Phys. J. **C54**, 577 (2008) and hep-ph/0709.3174.
- [7] C. Merino, M.M. Ryzhinski, and Yu.M. Shabelski, Eur. Phys. J. **C62**, 491 (2009); arXiv:0810.1275 [hep-ph]; arXiv:0906.2659 [hep-ph].
- [8] C. Merino, C. Pajares, M.M. Ryzhinskiy and Yu.M. Shabelski, Talk given at HSQCD Conf., St.Petersburg, 5-9 July 2010 and arXiv:1007.3206 [hep-ph].
- [9] A.B. Kaidalov, K.A. Ter-Martirosyan, and Yu.M. Shabelski, Yad. Fiz. **43**, 1282 (1986).
- [10] Yu.M. Shabelski, Z. Phys. **C38**, 569 (1988).
- [11] J. Dias de Deus and Yu.M. Shabelski, Yad. Fiz. **71**, 191 (2008).
- [12] V.A. Abramovsky, V.N. Gribov, and O.V. Kancheli, Yad. Fiz. **18**, 595 (1973).
- [13] A. B. Kaidalov, Sov. J. Nucl. Phys. **45**, 902 (1987); Yad. Fiz. **43**, 1282 (1986).
- [14] M. Froissart. Phys. Rev. **123** (1961) 1053.
- [15] K. A. Ter-Martirosyan, Phys. Lett. **B44**, 377 (1973).
- [16] ATLAS Collaboration, arXiv:1104.0326 [hep-ex].
- [17] K. Goulanos, arXiv:1105.4916 [hep-ph].
- [18] N.S. Amelin, N. Armesto, C. Pajares, and D. Sousa, Eur. Phys. J. **C22**, 149 (2001)
- [19] V.N. Gribov, Sov. Phys JETP **26**, 414 (1968).
- [20] V.A. Khose, A.D. Martin, and M. G. Ryskin, Eur. Phys. J. **C54**, 199 (2008); **C60**, 249 (2009).
- [21] E. Gotsman, E. M. Levin, U. Maor, and J.S. Miller, Eur. Phys. J. **C57**, 689 (2008).
- [22] S. Ostapchenko, arXiv: 1003.0196 [hep-ph].
- [23] V.A. Abramovsky, O.V. Kancheli, and I.D. Mandzhavidze, Yad. Fiz. **13**, 1102 (1971).
- [24] K. Aamodt et al., ALICE Collaboration, Eur. Phys. J. **C68**, 89 (2010) and arXiv: 1004.3034 [hep-ex].
- [25] K. Aamodt et al., ALICE Collaboration, Eur. Phys. J. **C68**, 345 (2010) and arXiv: 1004.3514 [hep-ex].
- [26] D. Ella, ALICE Collaboration, arXiv: 1102.2369 [hep-ex].
- [27] A.B. Kaidalov, Phys. Lett **B116**, 459 (1982).

- [28] K. Aamodt et al., ALICE Collaboration, arXiv: 1101.4110 [hep-ex].
- [29] H. Oeschler et al., ALICE Collaboration, arXiv: 1102.2745 [hep-ex].
- [30] CMS Collaboration, arXiv: 1102.4282 [hep-ex].
- [31] X. Artru, Nucl. Phys. B **85**, 442 (1975).
- [32] M. Imachi, S. Otsuki, and F. Toyoda, Prog. Theor. Phys. **52**, 346 (1974); **54**, 280 (1976); **55**, 551 (1976).
- [33] G.C. Rossi and G. Veneziano, Nucl. Phys. B **123**, 507 (1977).
- [34] D. Kharzeev, Phys. Lett. B **378**, 238 (1996).
- [35] V.G. Bornyanov et al., Uspekhi Fiz. Nauk. **174**, 19 (2004).
- [36] D. Diakonov, V. Petrov, and M. Polyakov, Z. Phys. **A359**, 305 (1997).
- [37] M.G. Ryskin and Yu.M. Shabelski, Eur. Phys. J. **C50**, 81 (2007) and hep-ph/0609222.
- [38] S.E. Vance, M. Gyulassy, and X-N. Wang, Phys. Lett. B **443**, 45 (1998).
- [39] E.M. Aitala *et al.*, E769 Collaboration, hep-ex/0009016; Phys. Lett. B **469**, 9 (2000).
- [40] B.Z. Kopeliovich and B. Povh, Z. Phys. C **75**, 693 (1997); Phys. Lett. B **446**, 321 (1999).
- [41] F. Bopp and Yu.M. Shabelski, Yad. Fiz. **68**, 2155 (2005) and hep-ph/0406158; Eur. Phys. J. A **28**, 237 (2006) and hep-ph/0603193.
- [42] G.H. Arakelyan, C. Merino, and Yu.M. Shabelski, Yad. Fiz. **69**, 911 (2006) and hep-ph/0505100; Phys. Atom. Nucl. **70**, 1110 (2007) and hep-ph/0604103; Eur. Phys. J. **A31**, 519 (2007) and hep-ph/0610264.
- [43] O.I. Piskounova, Phys. Atom. Nucl. **70**, 1110 (2007) and hep-ph/0604157.
- [44] V.V. Anisovich and V.M. Shekhter, Nucl. Phys. B **55**, 455 (1973).
- [45] A. Capella and C.A. Salgado, Phys. Rev. C **60**, 054906 (1999).
- [46] K. Aamodt et al., ALICE Collaboration, Phys. Rev. Lett. **105**, 072002 (2010) and arXiv:1006.5432 [hep-ex].
- [47] F. Dettori et al., LHCb Collaboration, Nucl. Phys. B (Proc. Suppl.) **206-207**, 351 (2010) and arXiv:1009.1221 [hep-ex].
- [48] A. Capella, A. Kaidalov, and J. Tran Thanh Van, Heavy Ion Phys. **9**, 169 (1999).
- [49] C. Merino, C. Pajares, and Yu.M. Shabelski, Eur. Phys. J. **C59**, 691 (2009) and arXiv:0802.2195 [hep-ph].